Simulation of the joining process of graded hardened multi-range capable rivets

Pia K. Holtkamp[1,a *], Christian R. Bielak[1,b], Mathias Bobbert[1,c] and Gerson Meschut[1,d]

[1]Laboratory for material and joining technology, Paderborn University, Paderborn, Germany

[a]holtkamp@lwf.upb.de, [b]bielak@lwf.upb.de, [c]bobbert@lwf.upb.de, [d]meschut@lwf.upb.de

Keywords: Self-Piercing Riveting, Versatile Joining, FEM, Heat Treatment

Abstract. The versatile self-pierce riveting (V-SPR) is a further development of semi-tubular self-pierce riveting. V-SPR enables adaptation to changing boundary conditions, such as a change in the material thickness combination, without varying the rivet die combination due to increased punch actuation and the use of multi-range capable rivets [1]. The inner punch first sets the rivet. The outer punch then forms the rivet head to the respective sheet thickness. For this, the rivet requires a hard shank and a ductile rivet head, which is achieved by an inductive local hardening process [2]. Until now, the joint formation of rivets with graded hardness profile has been challenging to estimate in the FEM simulation due to the inhomogeneous material conditions in the rivet. In this study, a method capable of reproducing the experimentally determined hardness levels of rivets in detail is shown. This FE model enables the realistic modelling of the mechanical properties of the rivet on the basis of the hardness profile in order to predict the correct deformation processes and stresses during the riveting process. First, the detailed experimental hardness mapping of the locally heat-treated rivets is transferred into the FE model. The FEM material model can predict the local strength of the rivet based on hardness by scaling the flow curves. To estimate the predictive capability of the FEM model, the joint formation of rivets with different graded hardness profiles is compared experimentally and simulative. Based on the validated model, the influence of different rivet hardness profiles on the joint formation is analysed numerically. By adapting the material model, a high level of correlation between the experiment's joint formation and the simulation can be achieved.

Introduction

The European Union has committed to significantly reducing CO_2 emissions by 2030 [3]. The automotive industry, one of the primary sources of CO_2 emissions, is a particular focus of attention. In order to reduce emissions, it is focussing on new drive concepts and lightweight construction strategies to reduce weight [4]. One standard method is multi-material construction, in which materials with different properties are combined in order to optimise the structure to the loads. As thermal joining processes are often unreliable with these material combinations, mechanical processes such as self-pierce riveting (SPR) are predominantly used.

Self-pierce riveting (SPR) enables the joining of different types of materials as two or more layered joints under the condition of accessibility from both sides. Four process steps characterise the continuous process sequence, see Fig. 1. The first step describes fixing the sheets using the blank holder. In the second step, the rivet is then fed through the punch, causing the rivet to penetrate the punch-side sheet metal and pierce it. The resulting slug is collected in the rivet shank. The third process step is characterised by the expansion and compression of the rivet and the resulting formation of the interlock. This creates a form- and frictional joint. And in the fourth process step, the tools retract and release the connection [5].

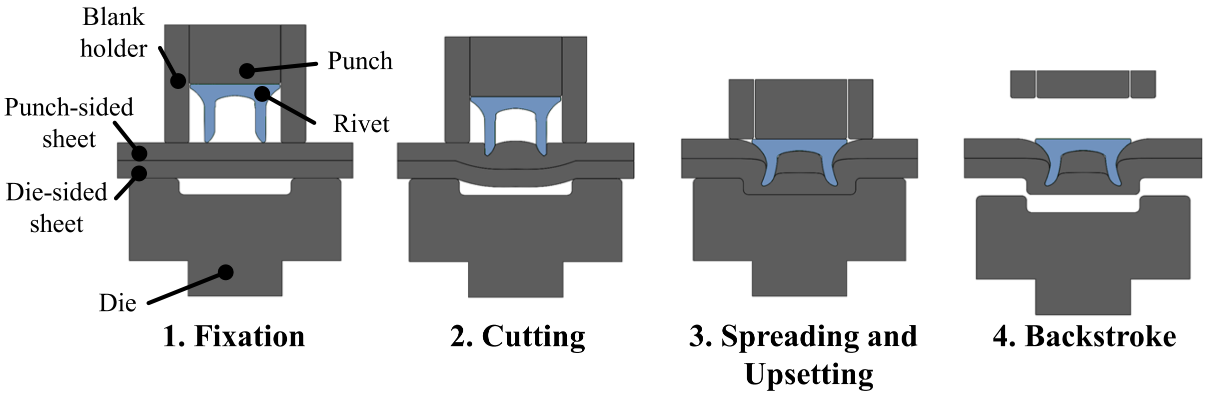

Figure 1 – Process sequence for self-pierce riveting (SPR) [5].

One restriction of SPR is the requirement to adapt the rivet-die combination to changing boundary conditions, such as a change in sheet thickness or the material used. For this reason, research is being carried out into more versatile and adaptable joining processes to enable an extended range of applications.

One approach to reducing rivet-die combinations is the use of a two-part die principle with a movable die element, which is demonstrated in [6]. This enables local overlapping of the joining zones with compressive stresses, which avoids cracks in die-cast aluminium components and extends the application of mechanical joining to brittle materials [7].

Another approach is versatile self-pierce riveting (V-SPR) [1]. This is characterised by an extended tool kinematics and a multi-range capable rivet, which increases the application range for different sheet thicknesses without requiring the rivet-die combination to be adapted. The process sequence is shown in Fig. 2.

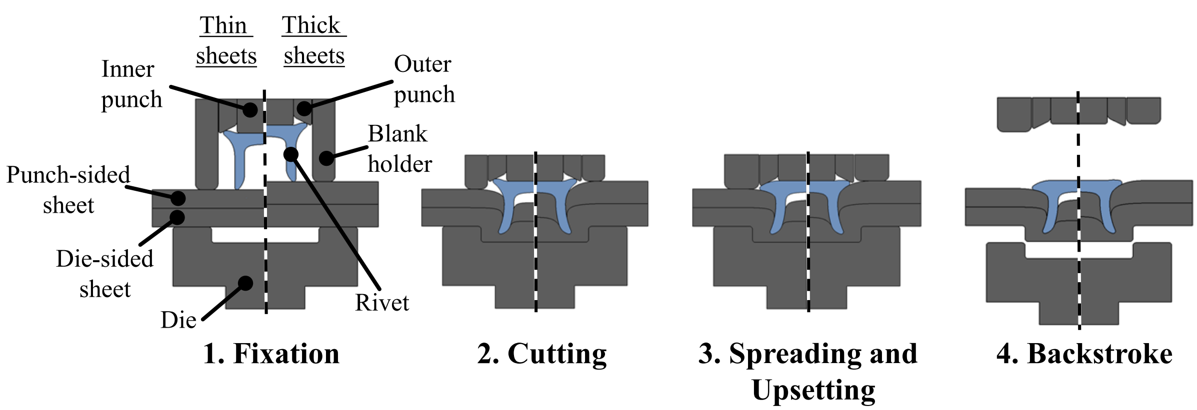

Figure 2 – Process sequence for V-SPR with head deformation [1].

The process sequence differs essentially from the SPR because of the split tool arrangement on the punch side, which consists of an inner and outer punch. The rivet is set by the inner punch, after which the outer punch enables the rivet head to be moulded to the respective sheet thickness. The multi-range rivets are currently manufactured by machining. Subsequent heat treatment ensures tempering to 480 HV, which corresponds to the H4 condition of conventional rivets [5].

Previous research into the V-SPR process has focussed on process development and joint formation. For aluminium joints in particular, a single rivet-matrix combination made it possible to join different material thicknesses [1]. Multi-material joints were also successfully realised [8]. However, the use of steel as a punch-sided material, especially in thin sheet thicknesses, proved to be problematic, as considerable deformation of the rivet head is required, which increases the risk of cracking. The rivet can be hardened by inductive localised heat treatment, which results in the rivet having a ductile head area for forming the rivet head protrusion and a stiff shank for punching the punch-side sheet. This study aims to transfer the inductively generated hardness grading of the rivet to the numerical simulation using a novel method to include different flow curves for the respective graded areas in LS-Dyna.

In previous studies, the respective degree of deformation within partitioned areas was specified for modelling locally different material states in the rivet and different material strengths were mapped using implemented flow curves [9]. In addition, the adjustment of graded rivet properties by the cold impact process was analysed, both numerically and experimentally [10]. In a study by [11], a two-part material approach was used for the numerical simulation of case-hardened flow-drill screws. The yield stress of the core material and the hardness values of the core and the outer layer were determined experimentally. The ratio of the Vickers hardness values between the hardened outer layer and the core was used to determine the yield stress of the hardened layer. The realistic modelling of the mechanical behaviour of the hardened layer was demonstrated by transferring the hardness values to the simulation through a correlation with the tensile strength. However, only two distinct hardness ranges were numerically modelled. In the following study, a continuous hardness grading over the entire geometry will be investigated.

Experimental procedure

The multi-range-capable rivet consists of the material C35 B+Cr. The aluminium alloy EN AW-6014 temper T4 with a sheet thickness of 1.0 mm on the punch side and a sheet thickness of 2.0 mm on the die side was selected. The chemical composition properties of the rivet material and the investigated materials EN AW 6014 and HCT590X are shown in Table 1.

Table 1 – Chemical composition properties of rivet material C35 B+Cr [12] and sheet materials EN AW-6014 temper T4 [13] and HCT590X [14].

Chemical composition C35 B+Cr (weight %)									
Elements	Si	C	Cu	Mn	P	S	Cr	Mo	B
Min.		0.35		0.60					0.0008
Max.	0.3	0.40	0.25	0.90	0.025	0.025	0.3	-	0.005
Chemical composition EN AW-6014, T4 (weight %)									
Elements	Si	Fe	Cu	Mn	Mg	Cr	Zn	Ti	V
Min.	0.30			0.05	0.40				
Max.	0.60	0.35	0.25	0.20	0.80	0.20	0.10	0.10	0.10
Chemical composition HCT590X (weight %)									
Elements	C	Si	Mn	P	S	Al	Cr+Mo	Nb + Ti	
Min.	0.15	0.75	2.5	0.04	0.015	0.15	1.4	0.15	

The localised heat treatment of the rivets is achieved using an inductive heating process. Fig. 3 shows the geometry of the multi-range capable rivet (a) and the experimental setup of the inductive local heat treatment (b). During induction heating, the rivets are placed on a chamotte rivet holder and fixed in the induction coil with a spring-loaded rod. The position of the rivet within the induction coil can be adjusted by setting the height of the device. In addition, the air supply enables targeted quenching of the rivets. By varying the holding times and temperatures as well as the positioning of the rivet in the induction coil, different local hardness profiles can be set within the rivet [2]. Hardness mapping is carried out using the Vickers hardness test to determine the hardness profile obtained. This represents the surface hardness profile of a sample as a 2D or 3D colour representation, as well as the HV values assigned to the x-y coordinates. The KB 30 S hardness testing machine from KB Prüftechnik GmbH is used for this purpose. This has an adjustable support table and a diamond pyramid as an indenter.

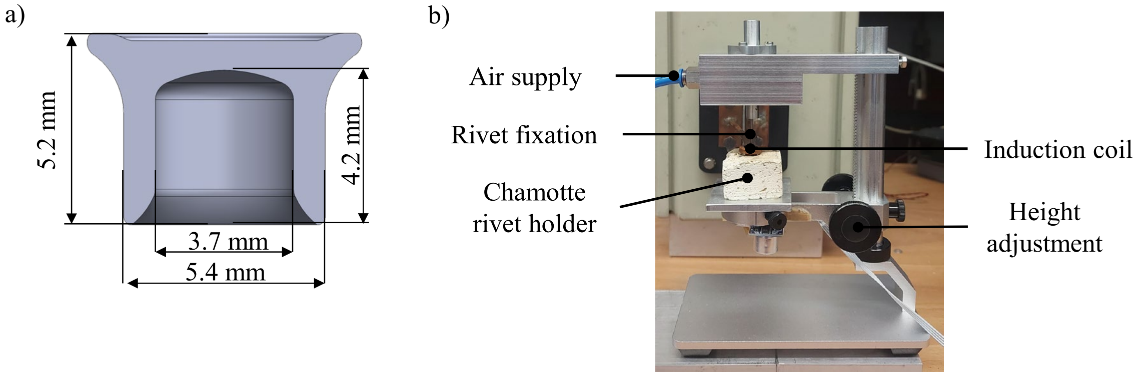

Figure 3 – Illustration of the rivet geometry (a), experimental set-up for local heat treatment by means of induction (b) [15].

In this study, two rivets with different graded hardness profiles are analysed, see Fig. 4. The parameters of the inductive local heat treatment of rivet A are a temperature of 860 °C with a holding time of 5 s and a subsequent quenching process by changing the coil position. The rivet B is heat treated at 860 °C with a holding time of 6 s without a subsequent quenching process [15]. These different heat treatment strategies allow different hardness profiles to be generated.

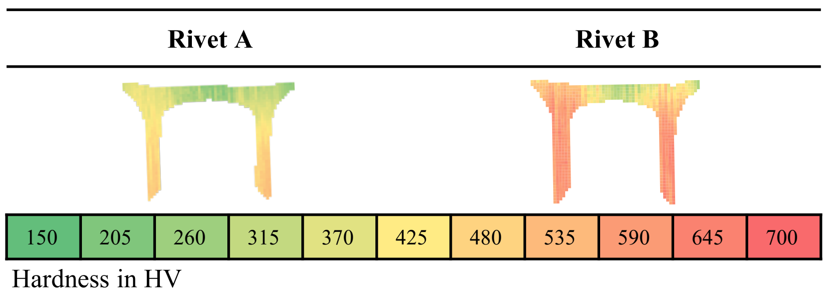

Figure 4 – Hardness Mapping of the multi-capable rivet with different graded hardness profiles [15].

Compression tests according to DIN 50106 [16] were carried out to determine the flow curve of the rivet material C35 B+Cr in the H4 condition [17]. The experimental data, see Fig 5 H4 exp., were extrapolated based on the ideal plastic material behaviour in the compression test using the mathematical approach according to Voce. In previous studies, an ideal plastic material behaviour of the 38B2 was also assumed [18]. The table in Fig. 5 was used to determine scaling factors for the flow curves of the different hardness grades based on the flow curve of the hardness grade H4 [5].

Materials Research Proceedings 54 (2025) 1413-1421 https://doi.org/10.21741/9781644903599-153

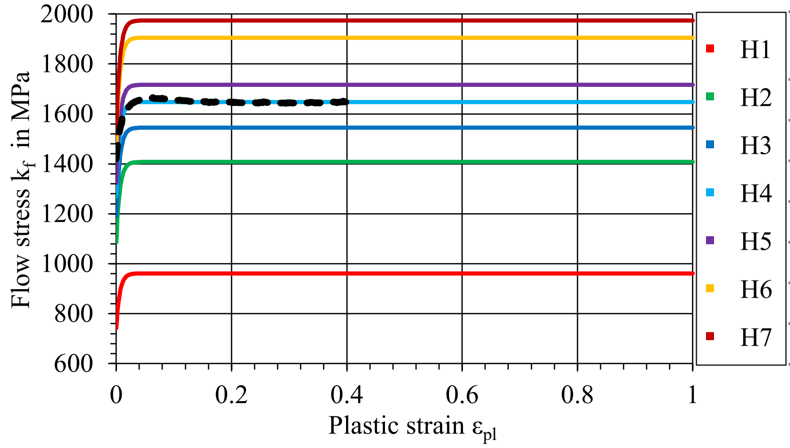

Hardness grade	HV	Scaling factor to H4
H1	280	0.583333333
H2	410	0.854166667
H3	450	0.9375
H4	480	1
H5	500	1.041666667
H6	555	1.15625
H7	575	1.197916667

Figure 5 – Flow curves of the rivet material C35 B+Cr in different hardness grades, the hardness grade in HV [5] and the scaling factor to H4.

For the joining process, a system is employed that allows independent movement of the inner and outer punches, as previously described. As shown in Fig. 6, the upper tool, comprising both punch components and a blank holder, and the lower tool are positioned within a column-guided frame [1].

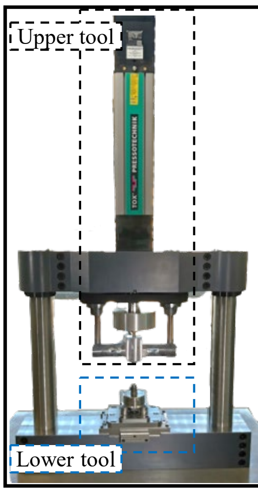

Drives
Servo-electric
Nominal force punches
80 kN
Drive (blank holder)
Pneumatic
Blank holder force
8 kN
Max. joining speed
80 mm/s
Measurement
Force and displacement

Figure 6 – Joining system with extended punch-sided tool actuator technology to process the multi-range capable self-piercing rivets [1].

Numerical simulation

To investigate the influence of different graded hardness profiles on the joint formation, a 2D axisymmetric simulation model, shown in shown in Fig. 7, was set up. This model is based on the preliminary investigations by Kappe *et al*. [19]. The FE model was developed using LS-Dyna simulation software and analysed through implicit calculation. The inner and outer punch are modelled as elastic components to facilitate a detailed analysis of the forces acting during the process. A displacement-controlled movement within the model is initiated through the constraint of the punch nodes. The die was also modelled as an elastic part, with its joining force measured in the lower area. The blank holder, modelled as a rigid part, applies a constant force throughout the experimental process. The material properties were implemented in the simulation model using the experimentally determined flow curves, which were presented for the sheet material and the rivet material in strength class H4 [17]. The contact behaviour between the rivet and the sheets, as well as the sheets themselves, was modelled using the static coefficient of friction of 0.2 [20]. The cutting of the punch-side sheet was realised using a geometric cutting criterion, induced by the process conditions.

FE-simulation – Relevant parameters	
Simulation software	LS-Dyna
Solver	smp_d_R910
Analysis	Implicit
Section	Shell
Element formulation	15 – Axissymmertric solid
Material seperation criterion	Geometrical
Process control	Displacement (Punches)
Punch feed direction	Y-Axis

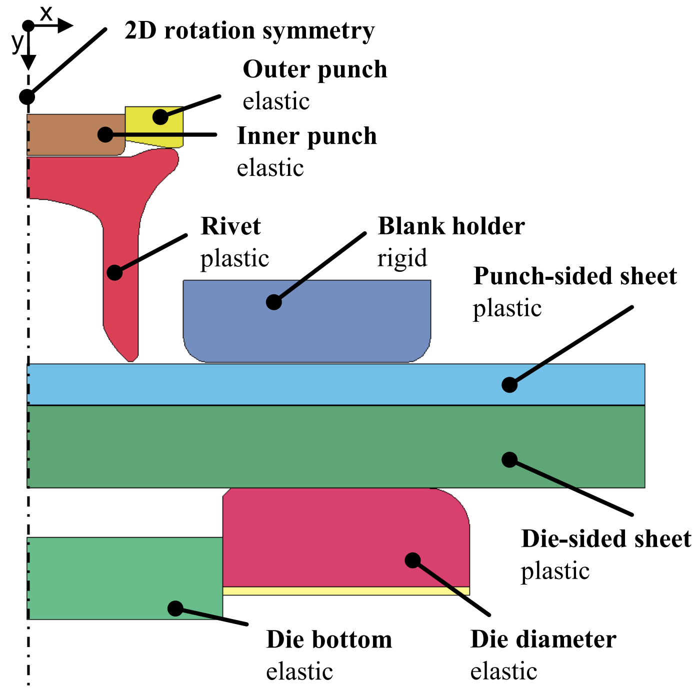

Figure 7 – Numerical setup of the V-SPR joining process.

The 2D simulation model is validated by comparing the micrograph and quality parameters of the joint formation of the multifunctional rivet with hardness H4, see Fig. 8. This shows very good agreement between the simulation and the micrograph. In particular, the flow behaviour of the rivet material is reproduced very well in the simulation.

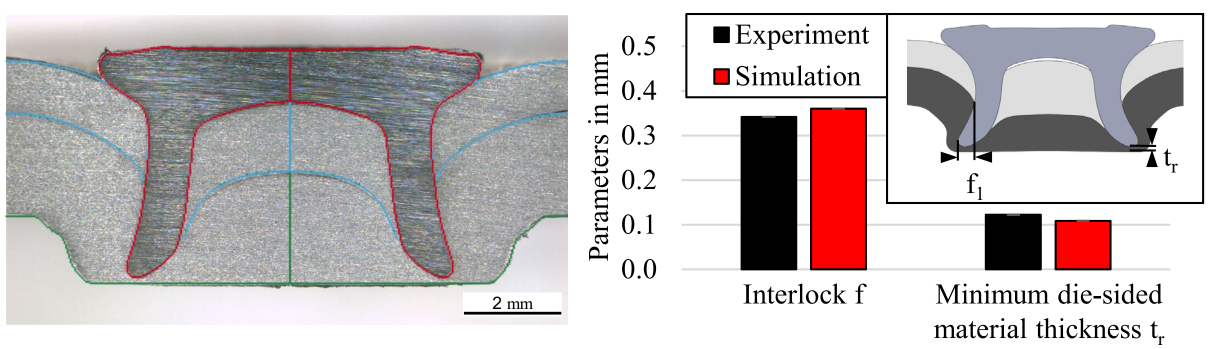

Figure 8 – Validation of the simulation model using the joint formation of the multifunctional rivet with hardness H4.

The graded hardness profile of rivet A and rivet B was transferred to the elements of the rivet in the simulation model using the experimentally determined hardness mapping. Based on the material model *MAT_TABULATED_JOHNSON_COOK, different hardness levels of the rivet material are assigned to the flow curves presented in Fig. 6. The flow curves are interpolated across the defined hardness ranges. By adapting the material model and the assumption that the different degrees of hardness are defined, a high level of correlation between the experiment's joint formation and the simulation can be achieved. Fig. 9 compares the micrographs and quality parameters of the joint formation of rivet A and rivet B with the results of the respective simulations.

The hardness grading of rivet A results in a properly formed joint according to the geometric parameters. Due to the hardness of the shank area, the rivet is able to cut through the sheet metal on the punch side and has sufficient ductility for spreading, resulting in the interlock. Rivet B has a higher hardness in the shank, which reduces the spreading behaviour, thereby reducing the interlock and the residual base thickness. The model prediction of rivet B shows a higher spreading behaviour of the rivet foot than the spreading behaviour in the experiment. One reason for this effect can be the low minimum die-sided material thickness of 0.01 mm to 0.02 mm in the experiment, which cannot be correctly mapped in the simulation due to the elements and re-meshing. Furthermore, a change in the influence of friction due to high stresses might be a reason for the deviation of the model prediction. The rivet head projection of rivet A has sufficient ductility for forming to the sheet metal on the punch side. The localised heating strategy of rivet B leads to a higher hardness profile in the rivet head projection. This leads to the formation of cracks in the rivet head projection during the forming process, which can be recognised in the micrograph. The FE model used cannot currently represent these cracks, therefore a suitable damage and failure material model of the rivet must be implemented.

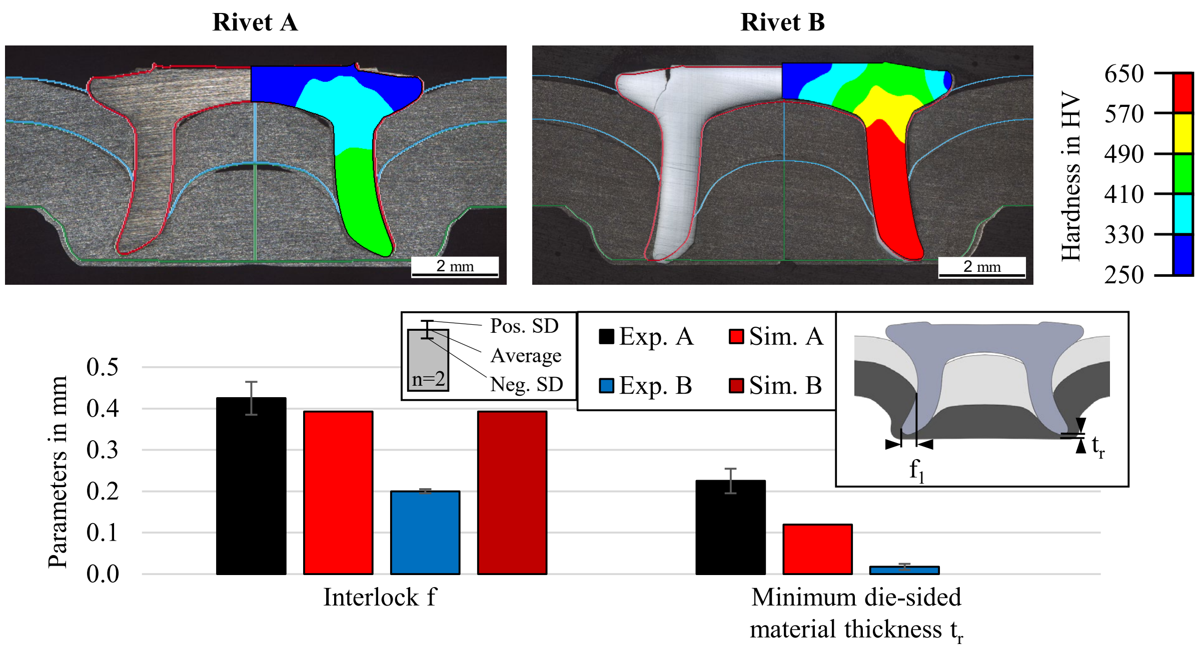

Figure 9 – Comparison of the joint formation of the experiment and the numerical simulation of rivets A and B.

In subsequent studies, the FE model is to be expanded to include a suitable damage model, which will enable the simulative modelling of cracks in the rivet. This FE model will be used to analyse different hardness grading of the rivet in other material combinations, in particular the use of the graded rivet in high-strength steel.

Summary

In this study, a method was presented that enables the experimentally determined hardness levels of rivets to be precisely modelled in the numerical simulation. The FE model allows a realistic representation of the mechanical properties of the rivet based on its hardness profile and maps the deformation mechanisms during the riveting process. For this purpose, the detailed hardness profile of the locally heat-treated rivets was first integrated into the FE model. The FEM material model reliably predicts the local strength of the rivets based on the hardness by scaling the flow curves. In subsequent studies, this method can be used to perform a numerical adjustment of the graded hardness profile of the rivet for different material combinations of the joining parts.

Acknowledgement
Funded by the Deutsche Forschungsgemeinschaft (DFG, German Research Foundation) – TRR 285/2 – Project-ID 418701707. The authors thank the German Research Foundation for their organisational and financial support. Data regarding the contents of the publication can be requested at www.trr285.de.

References

[1] F. Kappe, S. Wituschek, M. Bobbert, and G. Meschut, "Determining the properties of multi-range semi-tubular self-piercing riveted joints," Prod. Eng. Res. Devel., vol. 16, 2-3, pp. 363–378, 2022. https://doi.org/ 10.1007/s11740-022-01105-2

[2] F. Kappe, M. Bobbert, and G. Meschut, "Influence of local heat treatment of rivets on the joint formation of a versatile joining process," IOP Conf. Ser.: Mater. Sci. Eng., vol. 1307, no. 1, p. 12009, 2024. https://doi.org/ 10.1088/1757-899X/1307/1/012009

[3] European Commission. "Delivering the European Green Deal." [Online]. Available: https://commission.europa.eu/strategy-and-policy/priorities-2019-2024/european-green-deal/delivering-european-green-deal_en

[4] K. Martinsen, S. J. Hu, and B. E. Carlson, "Joining of dissimilar materials," CIRP Annals, vol. 64, no. 2, pp. 679–699, 2015. https://doi.org/ 10.1016/j.cirp.2015.05.006

[5] Technical Bulletin DVS 3410: Self-pierce Riveting - Overview., European Research Association for Sheet Metal Working, Düsseldorf, 2019.

[6] Donhauser G, Mauermann R, Quaißer G et al, "Stamping rivet upsetting tool comprises die endface which is radially divided into sectors outside raised area," DE19847980 A1.

[7] W. G. Drossel and M. Jäckel, "New Die Concept for Self-Pierce Riveting Materials with Limited Ductility," *KEM*, vol. 611-612, pp. 1452–1459, 2014. https://doi.org/ 10.4028/www.scientific.net/KEM.611-612.1452

[8] F. Kappe, S. Wituschek, M. Bobbert, M. Lechner, and G. Meschut, "Joining of multi-material structures using a versatile self-piercing riveting process," Prod. Eng. Res. Devel., vol. 17, no. 1, pp. 65–79, 2023. https://doi.org/ 10.1007/s11740-022-01151-w

[9] B. Uhe, G. Meschut, and M. Merklein, "Ressourcenschonende Herstellung von Halbhohlstanznieten durch Prozesskettenverkürzung," Dissertation, Shaker Verlag.

[10] C.-M. Kuball, "Grundlegende Untersuchungen zur umformtechnischen Herstellung von Halbhohlstanznieten aus hochverfestigenden Werkstoffen," 2024. https://doi.org/ 10.25593/978-3-96147-718-0.

[11] M. Costas, D. Morin, J. K. Sønstabø, and M. Langseth, "On the effect of pilot holes on the mechanical behaviour of flow-drill screw joints. Experimental tests and mesoscale numerical simulations," Journal of Materials Processing Technology, vol. 294, p. 117133, 2021. https://doi.org/ 10.1016/j.jmatprotec.2021.117133

[12] Saarstahl. "Werkstoff-Datenblatt Saarstahl C35R." Accessed: Feb. 12, 2024. [Online]. Available: https://www.saarstahl.com/sag/downloads/download/9082

[13] Novelis Global Automotive, Datasheet: Novelis AdvanzTM 6F - e170.

[14] Salzgitter Flachstahl GmbH. "Datenblatt: CR330Y590T-DP (HCT590X+Z*, HCT600XD, HC340XD**) CR330Y590T-DP (HCT590X+Z*, HCT600XD, HC340XD**): Mehrphasenstähle zum Kaltumformen – Dualphasenstähle." Accessed: Nov. 28, 2023. [Online]. Available: https://www.salzgitter-flachstahl.de/fileadmin/mediadb/szfg/informationsmaterial/produktinformationen/kaltgewalztes_feinblech/deu/hct590x.pdf

[15] P. Holtkamp, F. Kappe, P. Probst, M. Bobbert, and G. Meschut, "Investigation of local heat treatment strategies for a multi-range capable rivet and the influence on joint formation and load-bearing capacity," Proceedings of the Institution of Mechanical Engineers, Part L: Journal of Materials: Design and Applications, 2025, Art. no. 14644207241307508. https://doi.org/ 10.1177/14644207241307508

[16] Prüfung metallischer Werkstoffe: Druckversuch bei Raumtemperatur, 50106, DIN Deutsches Institut für Normung e. V, Berlin, Feb. 2023.

[17] F. Kappe, M. Bobbert, and G. Meschut, "New Approach for Versatile Self Piercing Riveting: Joining System and Auxiliary Part," KEM, vol. 883, pp. 3–10, 2021. https://doi.org/ 10.4028/www.scientific.net/KEM.883.3

[18] N. Karathanasopoulos and D. Mohr, "Strength and Failure of Self-Piercing Riveted Aluminum and Steel Sheet Joints: Multi-axial Experiments and Modeling," Journal of Advanced Joining Processes, vol. 5, p. 100107, 2022. https://doi.org/ 10.1016/j.jajp.2022.100107

[19] F. Kappe, C. Zirngibl, B. Schleich, M. Bobbert, S. Wartzack, and G. Meschut, "Determining the influence of different process parameters on the versatile self-piercing riveting process using numerical methods," Journal of Manufacturing Processes, vol. 84, pp. 1438–1448, 2022. https://doi.org/ 10.1016/j.jmapro.2022.11.019

[20] G. Meschut, O. Hahn, S. Horstmann, A. Esderts, and M. Sander, "Betriebsfestigkeit stanzgenieteter Bauteile: Ergebnisse eines Vorhabens der industriellen Gemeinschaftsforschung (IGF)," EFB-Forschungsbericht 429. Hannover: Europäische Forschungsgesellschaft für Blechverarbeitung e.V, 2016.